

# Spin current noise and Bell inequalities in a realistic superconductor-dot entangler

Olivier Sauret<sup>a,\*</sup>, Thierry Martin<sup>b</sup>, and Denis Feinberg<sup>a</sup>

<sup>a</sup> Laboratoire d'Etudes des Propriétés Electroniques des Solides,  
CNRS, BP 166,38042 Grenoble Cedex 9, France

<sup>b</sup>Centre de Physique Théorique, Université de la Méditerranée, Case 907, 13288 Marseille, France

Charge and spin current correlations are analyzed in a source of spin-entangled electrons built from a superconductor and two quantum dots in parallel. In addition to the ideal (crossed Andreev) channel, parasitic channels (direct Andreev and cotunneling) and spin flip processes are fully described in a density matrix framework. The way they reduce both the efficiency and the fidelity of the entangler is quantitatively described by analyzing the zero-frequency noise correlations of charge current as well as spin current in the two output branches. Spin current noise is characterized by a spin Fano factor, equal to 0 (total current noise) and  $-1$  (crossed correlations) for an ideal entangler. The violation of the Bell inequalities, as a test of non-locality (entanglement) of split pairs, is formulated in terms of the correlations of electron charge and spin numbers counted in a specific time window  $\tau$ . The efficiency of the test is analyzed, comparing  $\tau$  to the various time scales in the entangler operation.

PACS numbers: 73.23.Hk, 74.78.Na, 03.65.Ud

## I. INTRODUCTION

The production and the analysis of entangled states in condensed matter devices have recently emerged as a mainstream in nanoelectronics. Indeed, entanglement between electrons, besides checking fundamental quantum properties such as non-locality, could be used for building logical gates and quantum communication devices<sup>1</sup>. One may choose to consider nanoscopic devices where electrons behave essentially as free particles<sup>2</sup>, in a way similar to photons in quantum optics. Alternatively, exploiting electron interactions open new possibilities. This allows for instance to use the electron spin as a qubit in quantum dots<sup>3</sup>, owing to spin relaxation/coherence times ranging in semiconductors from fractions of  $\mu s$  (bulk<sup>4</sup>) to fractions of  $ms$  ( $T_1$  in quantum dots<sup>5</sup>). Spin entanglement<sup>6,7,8</sup> and teleportation<sup>9</sup> scenarios have been proposed within such a framework. A test of this spin entanglement was previously proposed with the help of a Bell diagnosis<sup>10</sup>, for a normal metal-superconducting device described within the context of scattering theory, operating in the ideal crossed Andreev regime<sup>11</sup>. However, in any device several unwanted electronic transitions may spoil entanglement and introduce decoherence. It is of key importance to check the device robustness against these parasitic effects and to show how to diagnose them through transport properties. Owing to the strategic role of entangled pairs in quantum information, we focus here on the source of spin-entangled electrons proposed by Recher et al.<sup>7</sup>. Following a detailed study of the average current due to the various processes<sup>12</sup>, the present work addresses noise correlations as a diagnosis of the device operation.

The entangler of Ref. 7 is made from a superconductor (S), adjacent to two small quantum dots in parallel, each being connected to a normal lead featuring a quantum channel. The dots are assumed to filter electrons one by one in a single orbital level, and Cooper pairs emit-

ted from the superconductor are split in the two dots – the so-called crossed Andreev channel (CA)<sup>14</sup>. Ideally, the constituent electrons then propagate in the two output leads as an entangled pair. Parasitic quantum processes may also occur in the entangler, they include elastic cotunneling (CT)<sup>14,15</sup> between the two dots via S, and tunneling of a pair through the same lead by a Direct Andreev process (DA) (Fig. 1). The main (CA) channel as well as DA were studied in Ref. 7. Using perturbation theory, the average current contributions to CA and DA were separately calculated. In the same spirit, Ref. 16 used a beam splitter on the entangler's output, in order to detect the entangled singlets by their noise bunching properties<sup>17</sup>. In reality, all these transport channels are mixed together. Instead of analyzing them separately, the full electron flow should be studied self-consistently, and be eventually characterized by its density matrix. The present work is based on a quantum master equation scheme which treats all processes on an equal footing<sup>12</sup> and gives access to the full density matrix of emitted electrons. It is used to compute the charge and spin correlations in the current flowing through the two branches of the entangler. In particular, spin current correlations<sup>18</sup>, even taken at zero frequency, are shown to quantify the entangler's efficiency and fidelity. Next, the violation of Bell inequalities (BI) can be tested by computing the cross correlators of charge and spin particle numbers in a given time window.

## II. IDEAL REGIME AND THE OTHER TRANSPORT PROCESSES

Transport is described by the processes connecting the different states – identified by the charge number and spin of the dots. Extra electrons  $n_1, n_2$  define the charge states ( $n_1 n_2$ ) in the dots. The electronic processes at work in the device include both coherent processes (CA,

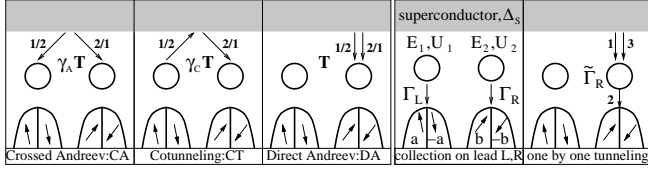


FIG. 1: Processes involved in the operation of the entangler. Pairs are emitted by the superconductor (gray) towards the two quantum dots, electrons are then collected by the leads  $L, R$  along predefined spin polarizations  $\pm a, \pm b$  ( $4^{th}$  panel). The order of elementary transitions involving virtual states is indicated : Crossed Andreev (CA) produce split pairs and triggers entanglement. CT (cotunneling), Direct Andreev (DA) as well as one-by-one tunneling through the same dot spoil entanglement. The three left panels describe coherent transitions, while the two right ones describe incoherent transitions.

CT and DA) and incoherent processes (transitions between the dots and the leads), see Fig. 1. In the ideal operation of this entangler, the Coulomb blockade prevents double occupancy in each dot, so that DA is forbidden. Also, the superconducting gap is supposed to be very large, so that one-by-one tunneling (last panel in Fig. 1) is also excluded. In addition, CT is neglected in this ideal regime, owing to the energy difference between the electron states on the two dots. Then, starting from an empty orbital state (denoted (00)), crossed Andreev (CA) reflection couples to a singlet state shared between the two dots,  $(11_s)$  with an amplitude  $\gamma_A T$  ( $\gamma_A \ll 1$  is the geometrical factor<sup>7,14,19</sup>). For a resonant CA transition, the dot energy levels  $E_i$  satisfy  $E_1 + E_2 = 0$ . The two electrons are collected into the leads (with chemical potentials  $\mu_{L,R} < E_1, E_2$ ) by transitions to states (01) or (10), then (00), with rates  $\Gamma_i$  ( $i = 1, 2$ ).

Let us now consider parasitic transport processes. If the intradot Coulomb charging energy  $U$  is not very strong, a coherent transition from (00) to a doubly occupied dot state (20) or (02) can occur via a direct Andreev (DA) process. Notice that this occurs with an amplitude  $T$  larger than for CA, since it is not affected by the geometrical reduction factor  $\gamma_A$ . Electrons are successively collected by a single lead, with rates  $\Gamma'_i$  then  $\Gamma_i$ , eventually reaching the empty state (00). This transport channel implies dot energies  $2E_i + U$ . In addition, DA can also start from an initial state (10) or (01), proceeding through states (21) (respectively (12)) with energies  $2E_1 + E_2 + U$  (respectively  $E_1 + 2E_2 + U$ ). Further collection into the leads either give states (20), (02), or singlet and triplet states  $(11_{s,t})$ . The mixing of triplet states with the desired singlets may cause decoherence in the source operation. In another process, the two electrons from a Cooper pair can tunnel one by one towards the same lead, involving a singly occupied virtual state which costs an energy at least equal to the superconducting gap  $\Delta_S$  (Fig. 1)). Contrary to the DA process, the dot is emptied before the quasiparticle in S is annihilated. The state (10) (or (01)) is reached by an incoherent process

with a rate  $\tilde{\Gamma}_i \sim \Gamma_i T_i^2 / \Delta_S^2$ . Last, CT involves a coherent transition of an electron from one dot to the other via S, and mixes all the above processes : it couples state (01) to (10), but also (20) (or (02)) to (11), (21) to (12). CT has an amplitude  $\gamma_C T \ll T$ , of the same order of magnitude as that of CA.

The density matrix equations involving populations (diagonal elements) and coherences (nondiagonal elements) include these processes altogether in a consistent and non-perturbative manner. Here one assumes weak couplings  $\Gamma_{L,R} < k_B \Theta$  of the dots to the output leads  $L, R$  ( $\Theta$  is the temperature). On the other hand, the leads are biased such as  $|\mu_{L,R}| > T$ ,  $\Gamma_{L,R}$ , ensuring irreversible collection of the electrons in  $L, R$ . The density matrix equations have been derived and detailed in Refs. 12,13, where the average currents in each branch have been computed. From these Bloch-like equations, one can also calculate the conditional probabilities – for a transition to a given state, assuming a previous initial state – which enter the calculations of the noise correlators<sup>20,21,22</sup>. Processes involving states with at most two electrons on the double dots are represented on Fig. 6 of Ref. 12, yet three-electron states are also included in the calculations.

### III. CHARGE AND SPIN CURRENT CORRELATIONS

Let us assume that the leads contain separate channels perfectly filtering spin currents polarized along two predefined and opposite directions. An understanding of the charge and spin correlations can be obtained by considering the spin-resolved zero-frequency noise<sup>18</sup> :  $I_\sigma$  being the current carried by electrons with spin  $\sigma = \pm a$  (along a given spin direction  $\mathbf{a}$ ), we define

$$S_{ij}^{\sigma\sigma'}(0) = \int dt \langle \{\Delta I_i^\sigma(t), \Delta I_j^{\sigma'}(0)\} \rangle, \quad (1)$$

where  $i, j = \{L, R\}$  and  $\Delta I_i^\sigma(t)$  is the deviation from the average current component  $\langle I_i^\sigma(t) \rangle = I_i^\sigma$ . We assume that the lead resistances and couplings to the dots are not spin-dependent. Because the superconductor is emitting singlet pairs, it results that the average current in each lead is not spin-polarized, e.g.  $I_i^\sigma = I_i/2$ . By definition, the charge and spin current noise correlation read:

$$S_{ij}^{ch} = \sum_\sigma (S_{ij}^{\sigma\sigma} + S_{ij}^{\sigma-\sigma}) \quad (2)$$

$$S_{ij}^{sp} = \sum_\sigma (S_{ij}^{\sigma\sigma} - S_{ij}^{\sigma-\sigma}). \quad (3)$$

The latter simply expresses the time correlations of the spin current  $I_i^{spin} = I_i^\sigma - I_i^{-\sigma}$ . The average total charge current passing through the entangler can be written as

$$I = I_L + I_R, \quad (4)$$

where the currents in leads  $L$  and  $R$  can be separated in two components, as

$$I_L = 2I_{LL} + I_{LR} , \quad (5)$$

$$I_R = 2I_{RR} + I_{LR} . \quad (6)$$

Here  $I_{LL}$ ,  $I_{RR}$  and  $I_{LR}$  respectively count pairs passing in unit time through  $L$ , or  $R$ , or through  $(L, R)$  as split (entangled) pairs. These current components can be written as:

$$I_{LR} = \frac{1}{2}p_S I , \quad (7)$$

$$I_{LL} = \frac{1}{2}p_L I , \quad (8)$$

$$I_{RR} = \frac{1}{2}p_R I , \quad (9)$$

with probabilities such that  $p_L + p_R + p_S = 1$ .

It is crucial to notice here that all the electrons passing through the entangler enter the two-dot system by pairs, emitted in an Andreev process (CA, DA or one-by-one tunneling). Therefore, the spin current fluctuations due to electrons of a given pair are correlated, since they track the passage of singlets. On the contrary, electrons emitted within different pairs display no spin correlation whatsoever. It results that, while calculating the correlations of spin currents at different times, the contributions of separate pairs drop out, so that spin noise in the leads uniquely tracks the spin correlations inside a pair. These correlations should be non-ideal since they track what remains from the emitted singlets after their passage through the two-dot system. This property of probing single pairs strongly contrasts with the charge current fluctuations which - in a sequential tunneling process - correlate successive pairs due to the Pauli principle and the Coulomb interaction in the dots. Therefore the spin current noise is very well suited to study the spin correlations inside pairs with zero-frequency noise. To illustrate this, it is convenient to write the various spin noise correlations as follows :

$$\begin{aligned} S_{LL}^{sp} &= 2eI_L - 4eI_{LL}(1 - f_L) = 2eI[p_L f_L + \frac{1}{2}p_S] , \\ S_{RR}^{sp} &= 2eI_R - 4eI_{RR}(1 - f_R) = 2eI[p_R f_R + \frac{1}{2}p_S] , \\ S_{LR}^{sp} = S_{RL}^{sp} &= -2eI_{LR}(1 - f_S) = -eI p_S (1 - f_S) . \end{aligned} \quad (10)$$

Let us comment the various terms in Eq. (10). The first term in  $S_{ii}^{sp}$  corresponds to the autocorrelation of electron wave packets<sup>18,20</sup>, and takes a Poisson value. The other terms are negative and reflect the spin anticorrelation inside singlets. The Fano-like reduction factors  $f_i$ ,  $f_S$  quantify this correlation. For instance, blocking one lead ( $\Gamma_R = 0$  for instance), all pairs pass through  $L$  ( $p_L = 1$ ) in a sequential way. In this case  $I = I_L = 2I_{LL}$ . Moreover, since the dot filters electrons one by one, one easily checks that  $f_L = 0$ , thus the spin noise through  $L$  is zero. This "spin Fano factor" equal to zero is a property of a S/N junction, characteristic of an unspoiled

Andreev process<sup>18</sup> : at a superconductor/normal (S/N) metal junction, zero spin noise is the fingerprint of charge carriers being paired in a singlet state. On the other hand, if the entangler operates ideally (only CA), then  $p_S = 1$ ,  $f_S = 0$  and  $S_{ii}^{sp} = eI$ . This is somewhat similar to the behaviour of a quantum dot in the sequential regime, with a single orbital state involved in transport and strong Coulomb charging energy, yielding a spin Fano factor equal to one<sup>18</sup>.

On the other hand, the crossed spin correlation is  $S_{LR}^{sp} = -eI$ . This value corresponds to an effective spin Fano factor  $-1$ , and serves as a reference value for an ideal operation of the device. These Poisson-like Fano factors, confirmed - see below - by the solution of the master equations, are valid for any value of the couplings of the dots to the leads. This is in contrast with the "charge" Fano factors in resonant quantum dot devices which reach the value one only in the very asymmetric limit, where correlations between successive charges crossing the dots become negligible.

Summing all contributions in Eq. (10), the spin noise of the total current is

$$S_{tot}^{sp} = S_{LL}^{sp} + S_{RR}^{sp} + S_{LR}^{sp} + S_{RL}^{sp} = 2eI F_S , \quad (11)$$

with the total spin Fano factor

$$F_S = p_L f_L + p_R f_R + p_S f_S . \quad (12)$$

Notice that in our definition the spin Fano factors measure the zero-frequency spin current noise in units of the average *charge* current (not the average spin current which is zero).

In the general case, when all (CA, DA and CT) processes come into play, pairs are both distributed (e. g. they exit through  $LL$ ,  $RR$  and  $LR$ ) and "mixed" together (electrons of a pair may intercalate between electrons of another) : for instance, due to states with three electrons in the double dot, two electrons of a split pair  $L, R$  can be separated by a time interval during which one or more pairs pass through a single dot (as illustrated by the sequence (00), (11), (10), (12), (11), (10), (00)). This variable delay between two spin-correlated electrons is responsible for the factors  $f_{L,R,S} > 0$  which measure the degree of mixing.

This preliminary analysis suggests that parasitic processes have two effects. First, they reduce the probability of split (entangled) pairs over non-entangled ones, thus  $p_S$  defines the entangler *efficiency*. And secondly, they reduce the spin correlation of a split pair,  $1 - f_S$  defining the entangler *fidelity* with respect to the singlet state. Notice that both efficiency and fidelity are defined here with respect to a given measurement probe, e. g. zero-frequency noise, or alternatively time-resolved correlation in the present work.

#### IV. QUANTITATIVE ANALYSIS

We now study these trends quantitatively. Charge and spin current noise correlations are calculated from the entangler quantum master equations, derived in ref. 12, where four-electron states in the dot pair are neglected for simplicity. We successively focus on the correlations of the total current  $I_L + I_R$ , of the separate currents  $I_L$ ,  $I_R$ , and on the crossed correlations between  $L$  and  $R$ .

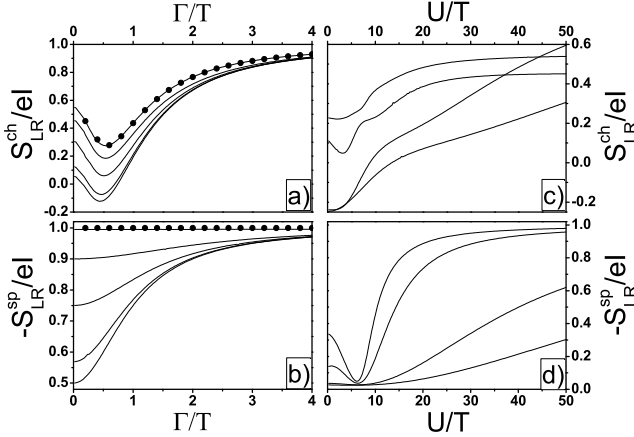


FIG. 2: Spin current cross-correlations, assuming CA to be resonant:  $E_1 + E_2 = 0$ , and  $\Gamma_L = \Gamma_R$ .  $\Delta_S$  is the largest energy scale, thus one-by-one tunneling is negligible.  $T = 1$  and  $\gamma_A = 0.2$  is assumed. In a) and b), only CA and CT are taken into account, assuming  $U \rightarrow \infty$ . Charge and spin cross-correlations are plotted for  $0 < \Gamma < 2$  and several values of  $E = |E_1 - E_2| = \{0, 0.2, 0.5, 1, 5\}$  (bottom to top). The dotted line features the ideal case. c) and d) correspond to  $0 < U < 50$  and  $E = 5$  (CA and DA, but no CT), for  $\Gamma_{L,R} = \{0.01, 1, 5, 10\}$  (top to bottom).

##### A. Ideal regime

Consider the ideal operation (CA only) for different values of  $\Gamma$  (assuming the Andreev amplitude to be equal to  $T = 1$ , and a geometrical factor  $\gamma_A = 0.2$ ). All electron pairs are split and cross the device sequentially (one after the other). The average (charge) current<sup>12</sup>  $I$  (see Fig. 4a) displays a maximum in the region  $\Gamma \sim \gamma_A T$ . This maximum can be easily explained by the balance between the entrance and exit rates of the two electrons in the double dot. The total charge noise through the entangler (see Fig. 5b, and also Ref. 13):

$$S_{tot}^{ch} = S_{LL}^{ch} + S_{RR}^{ch} + S_{LR}^{ch} + S_{RL}^{ch} \quad (13)$$

displays a minimum in the same range of parameters, as expected. Moreover, for large  $\Gamma/T$ , it reaches the value  $4eI$ . This doubling of the Fano factor with respect to the Poisson value signals the passage of electron pairs<sup>24</sup>. On the other hand, the crossed charge noise correlation  $S_{LR}^{ch}$

is positive (Fig. 2a), in contrast to the partition noise of single electrons, which is negative<sup>22</sup>. This reflects the perfect charge correlation of split pairs<sup>23</sup>. As a function of  $\Gamma/T$ ,  $S_{LR}^{ch}$  also displays a minimum (Fig. 2a) and becomes Poissonian in the limit  $\Gamma \gg \gamma_A T$ , where successive pairs are collected much faster than emitted, so are well-separated in time. Notice that in the ideal operation one has:

$$S_{LR}^{ch} = S_{LL}^{ch} = S_{RR}^{ch}. \quad (14)$$

Turning to the spin noise, one finds that the total spin noise  $S_{tot}^{sp}$  is zero, as discussed above. Moreover, one verifies that:

$$S_{LL}^{sp} = S_{RR}^{sp} = -S_{LR}^{sp} = eI, \quad (15)$$

thus diagnosing perfect spin correlations from the entangler.

##### B. General regime

Parasitic processes are next illustrated in presence of cotunneling alone ( $U$  and  $\Delta_S$  are chosen as infinite), which introduces a coupling between branches  $L$ ,  $R$ . In this case, pairs are distributed ( $LL$ ,  $RR$  and  $LR$ ) but still sequentially (they pass one after the other and do not mix) : therefore all the  $f$ 's in Eq. (1) are equal to zero. First, assuming  $\Gamma_L = \Gamma_R$ , the average current as well as  $S_{tot}^{ch}$  which sums over all branches are not modified<sup>25</sup>. On the contrary,  $S_{LR}^{ch}$  decreases (Fig. 2a) and can even become negative when cotunneling has a strong effect : due to branch coupling, charge cross-correlations are lost and partition noise may dominate over pair correlations. On the other hand, spin noise gives:

$$S_{ii}^{sp} = -S_{LR}^{sp} = eIp_s, \quad (16)$$

Therefore the spin Fano factor simply counts the split pairs (Fig. 2b) and measures the entangler efficiency. One checks that the total spin noise satisfies:

$$S_{LL}^{sp} + S_{RR}^{sp} + 2S_{LR}^{sp} = 0, \quad (17)$$

i. e. the whole entangler is a perfect Andreev source : whatever the origin of the pairs ( $LL$ ,  $RR$  or  $LR$ ), they are well-separated and the spin correlations of successive electrons is perfect. Notice that  $p_s$  tends to one for large  $\Gamma \gg \gamma_C T$  where CT has no time to occur and becomes irrelevant. In practice, for large  $|E_1 - E_2|/T > 5$ , CT is merely suppressed. In summary, with CT alone we have a situation where the efficiency of the entangler is reduced (and measured by the spin noise), while its fidelity remains perfect. Yet, notice that further use of these pairs in the output quantum channels would require an additional device to collect split pairs  $LR$  and filter out the others.

Next, double occupancy in the dots is allowed (process DA). Fixing  $\Gamma/T$ , the crossed charge noise is reduced and

can become negative at small  $U$  (Fig. 2c). Spin noise correlations also decrease as  $U/T$  decreases (Fig. 2d). The structures observed at small  $U$  for small  $\Gamma$  are due to the difference between the single electron levels  $E_1$ ,  $E_2$ , and DA transitions becoming resonant when  $E_i \sim -U$ . The width of the minimum increases for large  $\Gamma$ , due to two competing processes. On one hand, the probability for having a split pair (CA) in the 2 dots oscillates on a large time scale  $(\gamma_A T)^{-1}$ . On the other hand, the probability for a DA processes is smaller, but it oscillates more rapidly<sup>12</sup> ( $(U^2 + 4T^2)^{-1/2}$ ). A high detection rate thus dynamically favors the fast DA process, even though it is weaker. In the resonant regime  $E_i \sim -U$ ,  $S_{LL}^{ch}$  can even approach  $4eI_L$ , e.g. noise doubling in branch  $L$ . Moreover, it is important to point out that due to direct Andreev processes, the total spin noise is no more equal to zero. Actually, the occurrence of three-electron states in the double dot has the effect of mixing the pairs, reducing the fidelity, especially for small  $U$  and  $\Gamma$ .

In summary, the analysis of this quite general case demonstrates that optimal pair correlations are obtained if  $\gamma_A T < \Gamma < U$ . Nevertheless, at fixed  $\Gamma/U$ , a too small  $\gamma_A T/\Gamma$  ratio is detrimental, as it favours  $LL$  and  $RR$  pairs by a dynamical effect.

## V. BELL INEQUALITY TEST

In quantum optics, entanglement is typically probed by a Bell inequality (BI) test. It relies on the measurement<sup>26</sup> of number correlators. One may simplify the response of the electronic circuit such as to measure, not the instantaneous current, but instead the particle number accumulated during a time  $\tau$  is:

$$N_\alpha(t, \tau) = \int_t^{t+\tau} dt' I_\alpha(t') , \quad (18)$$

( $\alpha = \pm a, \pm b$  see Fig. 1). The inequality which is derived assuming a product density matrix weighted by local hidden variable reads<sup>11</sup>:

$$|G(\mathbf{a}, \mathbf{b}) - G(\mathbf{a}, \mathbf{b}') + G(\mathbf{a}', \mathbf{b}) + G(\mathbf{a}', \mathbf{b}')| \leq 2, \quad (19a)$$

$$G(\mathbf{a}, \mathbf{b}) = \frac{\langle (N_a(\tau) - N_{-a}(\tau))(N_b(\tau) - N_{-b}(\tau)) \rangle}{\langle (N_a(\tau) + N_{-a}(\tau))(N_a(\tau) + N_{-a}(\tau)) \rangle} \quad (19b)$$

In Ref.11, the correlators  $\langle N_\alpha(\tau)N_\beta(\tau) \rangle$  were related to zero-frequency current noise correlators via an approximate relation. This approximation breaks down for short times. We follow Ref.27 and calculate the correlators from first principles. The cross correlator for arbitrary spin directions of the filters can be separated into a parallel and an antiparallel component:

$$\begin{aligned} \langle N_\alpha(\tau)N_\beta(\tau) \rangle &= \langle N_{L\uparrow}(\tau)N_{R\downarrow}(\tau) \rangle \sin^2(\theta_{\alpha\beta}/2) \\ &+ \langle N_{L\uparrow}(\tau)N_{R\uparrow}(\tau) \rangle \cos^2(\theta_{\alpha\beta}/2) \end{aligned} \quad (20)$$

with  $\theta_{\alpha\beta}$  the relative angle between the polarizations in  $L$  and  $R$ . With the same choice of angles as considered

in Ref. 11 the BI becomes:

$$|\Delta N_{LR}^{sp}/(\Delta N_{LR}^{ch} + \Lambda^+)| \leq 1/\sqrt{2} \quad (21)$$

with

$$\Delta N_{LR}^{sp} = \langle N_{L\uparrow}(\tau)N_{R\downarrow}(\tau) \rangle - \langle N_{L\uparrow}(\tau)N_{R\uparrow}(\tau) \rangle , \quad (22)$$

and

$$\Delta N_{LR}^{ch} + \Lambda^+ = \langle N_{L\uparrow}(\tau)N_{R\downarrow}(\tau) \rangle + \langle N_{L\uparrow}(\tau)N_{R\uparrow}(\tau) \rangle , \quad (23)$$

where

$$\Lambda^+ = \tau^2 \langle I_L \rangle \langle I_R \rangle \quad (24)$$

is the reducible part of the charge correlator.

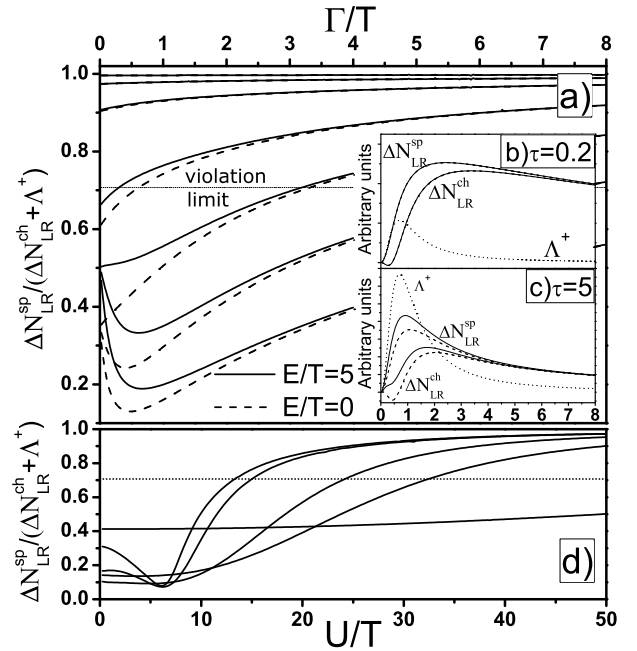


FIG. 3: The left part of the BI is compared to the limit  $2^{-1/2}$  (one assumes  $T = 1$  and  $\gamma_A = 0.2$ ). a) It is plotted for  $0 < \Gamma_{L,R} < 8$ , two values of  $E$  (0, and 5 which simulates the ideal working regime), and  $\tau T/h = \{0.2, 0.5, 1, 5, 10, 20\}$  (from the top to the bottom). To characterize the BI test, each contribution of  $|\Delta N_{LR}^{sp}|/(\Delta N_{LR}^{ch} + \Lambda^+)$  is plotted for  $\tau = 0.2$  b),  $\tau = 5$  c). d) Double occupancy is taken into account, assuming  $E = 5$ ,  $\Gamma_{L,R} = \{0.01, 1, 5, 10, 100\}$  (top to bottom) and  $\tau = 0.2$

In the ideal case (see Fig. 3a), the BI violation is maximal for  $\tau < h/T$  ( $h$  is the Planck constant). Increasing  $\tau$ , thus the number of measured pairs, quantum spin correlations show a minimum at  $\Gamma \sim \gamma_A T$ , due to a decrease of  $\Delta N_{12}^{sp/ch}/\Lambda^+$  (Fig. 3b,c). BI violation is recovered provided  $\Delta N_{12}^{ch} \sim \tau I$  dominates over  $\Lambda^+ = \tau^2 I^2$ , where  $I \sim \gamma_A^2 T^2/\Gamma$  for large  $\Gamma$  and  $I \sim \Gamma$  for small  $\Gamma$ . This means that pairs should be measured roughly one by

one<sup>11</sup>. Now, considering parasitic processes, CT tends to prevent BI violation at small  $\Gamma$ , and for large enough  $\tau$  (Fig. 3a). Finite  $U$  sensibly decreases the quantum spin correlations (Fig. 3d). The minimum flattens as  $\Gamma$  increases, as in Fig. 2d (dynamical effect). Yet, comparing Figs. 2 and 3, one sees that the BI test is much less affected by parasitic processes than the spin noise. For instance, with  $\Gamma = 5$  and  $U/T = 40$ , the spin noise is about 0.5, signalling a low efficiency, while the BI is violated with  $\tau = 0.2$ . In fact, this window allows filtering of split CA pairs, mostly dropping "wrong" DA pairs. Therefore, tuning  $\tau$  to an optimum value yields high fidelity of entanglement, even if the efficiency of the entangler is low.

## VI. SPIN-FLIP PROCESSES

Finally, let us address the effect of spin-flip scattering in the dots, here simply described by a spin relaxation time  $\tau_{sf}$ . As entanglement is concerned, this acts as a decoherence source, as it induces some mixing of singlet states ( $11_s$ ) with triplet states ( $11_t$ ). Spin-flip is easily incorporated into the general density matrix equations<sup>13</sup>, in a way similar to Ref. 18. It consists in defining occupation states ( $n_{1\sigma}, n_{2\sigma}$ ), and adding into the density matrix equations the terms corresponding to the decay of the spin densities  $n_{i\sigma} - n_{i-\sigma}$ . The effect of spin relaxation is summarized on Fig. 4. First, surprisingly enough, the average current is strongly quenched as soon as the spin-flip rate is of the order of the CA amplitude (Fig. 4a). This can be explained as follows. CA is coherent provided it involves a spin-conserving transition between degenerate states. Spin-flip in the dot, if faster than the CA resonance between states (00) and ( $11_s$ ), suppresses this resonance, opening a new decay channel. Indeed, spin flip competes with CA in a way similar to charge decay toward  $L, R$ . For  $\tau_{sf} < h/\Gamma < h/\gamma_A T$ , the current behaves as  $\tau_{sf}^2$ . For the same reasons, spin-flip also decreases charge correlations (Fig. 4b). Secondly, as expected, spin-flip decreases the spin noise correlations in leads  $L, R$  (Fig. 4b), by essentially diminishing the fidelity  $1 - f_S$ . In addition, Bell correlations are also affected by spin-flip, but, as above, much less than spin noise.

## VII. DISCUSSION

Let us now discuss the relevance of the above analysis in view of a future experimental realization of this entangler. First, we summarize the required operation regime, from the above as well as previous discussion<sup>7,12</sup> :

$$\begin{aligned} \Delta_S, U, |E_1 - E_2| &> \delta\varepsilon > \mu_{L,R}, k_B\Theta, \tau_{sf}^{-1} \\ &> \Gamma_{L,R} > \gamma_A T, \gamma_C T \end{aligned} \quad (25)$$

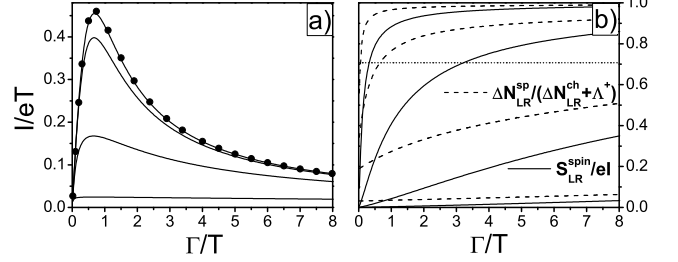


FIG. 4: (a) Average current  $I$  ; (b) spin current noise (continuous) and Bell correlation (dotted), as a function of  $\Gamma/T$ , with  $U = \infty, E = 5$  (CA only) and finite spin-flip time  $\tau_{sf}$  in the dots.  $\tau_{sf} T/h = \{10, 1, 0.1, 0.01\}$  decreases from top to bottom.

where  $\mu_{L,R}$  is the voltage drop between the superconductor and the leads  $L, R$  and  $\delta\varepsilon$  the separation between different orbital states in the dots. We assume that the average currents in both leads can be measured, as well as zero-frequency (charge and spin) noise correlations. Niobium will be taken for the superconductor ( $\Delta_S \sim 9.2K$ ), and  $\delta\varepsilon \sim 1meV \sim 12K$  for GaAs or InAs-based small quantum dots. A reasonable value for  $U$  is  $45K$ , larger than  $\Delta_S$ , which does not change the above conclusions, for which  $U < \Delta_S$  is instead assumed. A typical relaxation rate is  $\Gamma_{L,R} \sim 100mK$ , larger than  $k_B\Theta$ . One can then discuss the operation of the entangler as a function of the CA amplitude, say the parameters  $T$  and  $\gamma_A$ . As an experimental constraint, we fix the value of the current to a minimum of  $1pA$ , to make current correlations measurable. The current is plotted in Fig. 5a in nanoAmperes as a function of the electronic amplitude  $T$ , expressed in Kelvins, for two values of  $\gamma_A$ .

For optimum operation, the entangler should provide pairs which are i) well-separated in time; ii) split as much as possible in  $(L, R)$ ; iii) in the singlet state. As a first probe, the total charge noise tests the temporal separation of successive pairs, signaled by the doubling of shot noise,  $S_{tot}^{ch} = 4eI$  (Poisson result). We have numerically verified (see Fig. 5b) that this criterion is fulfilled up to a few percent if  $\gamma_A T \leq \Gamma_{L,R}$ . It is compatible with our constraint on  $I$  for  $T \sim 0.1K$  ( $\gamma_A = 0.01$ ) and  $T \sim 0.01K$  ( $\gamma_A = 0.2$ ).

As a second probe, the total spin noise also reflects the "mixing" of pairs in time, being zero if pairs are well-separated ( $T \leq \Gamma$  whatever  $\gamma_A$  without spin flip). Fig. 5c shows that this criterion is very well fulfilled (lower curve). In addition,  $S_{tot}^{sp}$  is sensitive to spin-flip. Therefore a combination of total charge and spin noise gives information on pair mixing and spin flip. Spin flip tends to increase  $S_{tot}^{sp}$  from the ideal value 0, especially for large  $\gamma_A$ .

As a third criterion, crossed spin correlations provide information on the fraction  $p_S$  of split pairs  $(L, R)$ . We find that  $\gamma_A = 0.2$  gives an excellent ratio (nearly 1 for  $T \leq \Gamma_{L,R}$ ). On the contrary, for  $\gamma_A = 0.01$ , this ratio

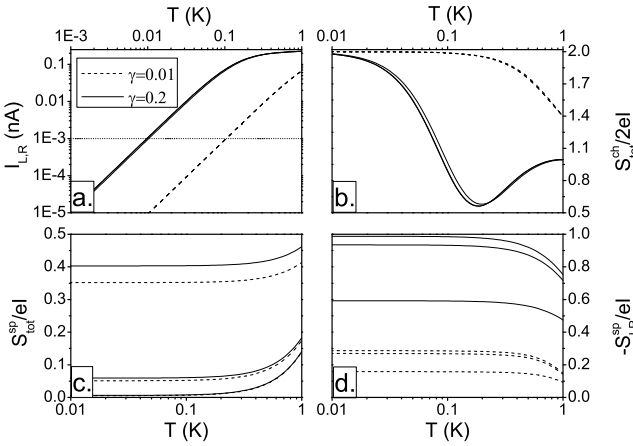


FIG. 5: Various diagnosis of the entangler, plotted as function of the pair tunnel amplitude  $T$  (in Kelvins), for  $\gamma_A = 0.01$  and  $0.2$ . a) The average current, assumed larger than  $1 \text{ pA}$ ; b) The total charge noise; c) The total spin noise. The spin-flip time decreases from bottom to top,  $\tau_{sf}(\text{ns}) = \{100, 10, 1\}$ ; d) The crossed spin noise. The spin-flip time decreases from top to bottom,  $\tau_{sf}(\text{ns}) = \{100, 10, 1\}$ , causing nearly no variation in panels a,b.

drops to about 0.2, *LL* and *RR* pairs being "dynamically" favored. Unless some further processing of pairs is achieved, this is detrimental to the entangler operation.

To summarize this analysis, a small value of  $\gamma_A$  is preferable for pair separation, but a large one is requested for the singlet fidelity. Given these conflicting requirements, a good compromise is obtained with large  $\gamma_A \sim 0.2$  but small  $T \sim 0.01K$ . Concerning the spin-flip time, values of the order of  $h/T \sim 50\text{ns}$  are acceptable.

### VIII. CONCLUSION

We have analyzed in detail the operation of a realistic superconductor-dot entangler. We have shown that

zero frequency charge and spin current correlations allow a detailed analysis of the efficiency and fidelity of the entangler in terms of parasitic and spin flip processes. Spin Fano factors for spin current correlations appear as an optimum characterization of the entangler operation. Due to the absence of spin correlation of electrons emitted within different Andreev processes, such spin Fano factors directly probe the spin correlations within an entangled pair. Depending on the quantity under interest, they are equal to  $\pm 1$  in the ideal operation regime. In this sense, measuring the spin current noise is an alternative to time-resolved measurements which should capture pairs one by one. Yet, for an absolute diagnosis of entanglement, a time-resolved Bell inequality measurement is necessary, within a narrow enough time window. Contrarily to low frequency measurements, this allows to check the entangler fidelity even in presence of a low efficiency. As a result of this work, we conclude that a satisfactory operation is upon reach with realistic parameters. For detection rates  $\Gamma \sim 100mK$ , the shortest time window described for a Bell test corresponds to  $\tau \sim 1ns$ , a time scale which could be accessible with fast electronics apparatus. Moreover, the geometric parameter  $\gamma_A$  appears to be crucial and should be rather large. Encouraging results have recently been obtained in two experiments which have observed crossed Andreev reflections at distances not very small compared to the superconductor coherence length<sup>28</sup>.

LEPES is under convention with Université Joseph Fourier. Further support from Ministry of Research "A.C. Nanosciences NR0114" is gratefully acknowledged.

\* Present address : Department of Theoretical Physics, Budapest University of Technology and Economics, Budapest, Hungary.

<sup>1</sup> M. A. Nielsen and I. L. Chuang, *Quantum Computation and Quantum Information* (Cambridge University press, 2000).

<sup>2</sup> C. W. J. Beenakker, C. Emery, M. Kindermann and J. L. van Velsen, *Phys. Rev. Lett.* **91**, 147901 (2003); C. W. J. Beenakker and M. Kindermann, *Phys. Rev. Lett.* **92**, 056801 (2004); P. Samuelsson, E. V. Sukhorukov and M. Büttiker, *Phys. Rev. Lett.* **91**, 157002 (2003); P. Samuelsson, E.V. Sukhorukov, M. Büttiker *Phys. Rev. Lett.* **92**, 026805 (2004).

<sup>3</sup> D. Loss and D. P. DiVincenzo, *Phys. Rev. A* **57**, 120 (1998).

<sup>4</sup> J. M. Kikkawa and D. D. Awschalom, *Phys. Rev. Lett.* **80**, 4313 (1998).

<sup>5</sup> J. M. Elzerman, R. Hanson, L. H. W. van Beveren, B. Witkamp, L. M. K. Vandersypen and L. P. Kouwenhoven,

*Nature* **430**, 431 (2004).

<sup>6</sup> G. B. Lesovik, T. Martin, and G. Blatter, *Eur. Phys. J. B* **24**, 287 (2001).

<sup>7</sup> P. Recher, E. V. Sukhorukov, and D. Loss, *Phys. Rev. B* **63**, 165314 (2001).

<sup>8</sup> W. D. Oliver, F. Yamaguchi, and Y. Yamamoto, *Phys. Rev. Lett.* **88**, 037901 (2002). D. S. Saraga, D. Loss, *Phys. Rev. Lett.* **90**, 166803 (2003).

<sup>9</sup> O. Sauret, D. Feinberg and T. Martin, *Eur. Phys. J. B* **32**, 545 (2003); O. Sauret, D. Feinberg and T. Martin, *Phys. Rev. B* **69**, 035332 (2004).

<sup>10</sup> S. Kawabata, *J. Phys. Soc. Japan* **70**, 1210 (2001).

<sup>11</sup> N. M. Chtchelkatchev, G. Blatter, G. B. Lesovik and T. Martin, *Phys. Rev. B* **66**, 161320(R) (2002).

<sup>12</sup> O. Sauret, D. Feinberg and T. Martin, *Phys. Rev. B* **70**, 245314 (2004).

<sup>13</sup> O. Sauret, PhD Thesis, Université Joseph Fourier, Grenoble (2004, in French).

<sup>14</sup> G. Deutscher and D. Feinberg, *Appl. Phys. Lett.* **76**, 487 (2000); G. Falci, D. Feinberg, and F. W. J. Hekking, *Europhys. Lett.* **54**, 255 (2001); D. Feinberg, *Eur. Phys. J.B* **36**, 419 (2003).

<sup>15</sup> D. V. Averin and Yu. V. Nazarov, in *Single Charge Tunneling*, H. Grabert and M.H. Devoret eds. (Plenum, New York 1992).

<sup>16</sup> P. Samuelsson, E.V. Sukhorukov and M. Büttiker *Phys. Rev. B* **70**, 115330 (2004).

<sup>17</sup> G. Burkard, D. Loss, and E. V. Sukhorukov *Phys. Rev. B* **61**, R16303-R16306 (2000). G. Burkard and D. Loss *Phys. Rev. Lett.* **91**, 087903 (2003).

<sup>18</sup> O. Sauret and D. Feinberg, *Phys. Rev. Lett.* **92**, 106601 (2004).

<sup>19</sup> M. S. Choi, C. Bruder and D. Loss, *Phys. Rev. B* **62**, 13569 (2000).

<sup>20</sup> A. N. Korotkov *Phys. Rev. B* **49**, 10381-10392 (1994);

<sup>21</sup> The initial conditions for calculating correlations functions within the density matrix equations should be specified for the coherences as well as for the populations. At  $t = 0$  the latter are taken as usual to be 1 for one (arbitrary) state and 0 for the others. On the other hand, the coherences are naturally taken to be zero at  $t = 0$ .

<sup>22</sup> Ya. M. Blanter and M. Büttiker, *Physics Rep.* **336**, 1 (2000).

<sup>23</sup> J. Torrès and T. Martin, *Eur. Phys. J. B* **12**, 399 (1999).

<sup>24</sup> V. A. Khlus, *Zh. Éksp. Teor. Fiz.* **93**, 2179 (1987) [Sov. Phys. JETP **66**, 1243 (1987)]; X. Jehl, P. Payet-Burin, C. Baraduc, R. Calemczuk and M. Sanquer, *Phys. Rev. Lett.* **83**, 1660 (1999).

<sup>25</sup> This is not true anymore if the two branches are unbalanced, e.g.  $\Gamma_L \neq \Gamma_R$ .

<sup>26</sup> A. Aspect, J. Dalibard, and G. Roger, *Phys. Rev. Lett.* **49**, 1804 (1982); A. Zeilinger, *Rev. Mod. Phys.* **71**, S288 (1999).

<sup>27</sup> A.V. Lebedev, G.B. Lesovik and G. Blatter, *Phys. Rev. B* **71**, 045306 (2005).

<sup>28</sup> D. Beckmann, H. B. Weber and H. v. Löhneysen, *Phys. Rev. Lett.* **93**, 197003 (2004); S. Russo, M. Kroug, T. M. Klapwijk and A. F. Morpurgo, unpublished (arXiv:cond-mat/0501564).